THE ASTROPHYSICAL JOURNAL, 355:114–129, 1990 May 20

ULTRAVIOLET INTERSTELLAR ABSORPTION TOWARD HD 163522, A HALO STAR AT 9 KILOPARSECS IN THE DIRECTION $l = 350°$ AND $b = -9°$

BLAIR D. SAVAGE,[1,2] DERCK MASSA,[2,3] AND KENNETH SEMBACH[1]

Received 1989 July 5; accepted 1989 November 27

ABSTRACT

UV interstellar absorption line measurements obtained by the *IUE* satellite toward HD 163522 in the direction $l = 349.^{\circ}6$ and $b = -9.^{\circ}1$ are analyzed. The UV stellar spectrum of HD 163522 is consistent with the B1 Ia MK classification which implies a distance of $9.4^{+2.4}_{-1.9}$ kpc, placing the star beyond the Galactic center at a distance away from the Galactic plane of $z = -1.5$ kpc. By combining four short-wavelength spectra and two long-wavelength spectra, we have produced an absorption-line spectrum with S/N ≈ 15–25. The UV interstellar absorption lines for neutral, weakly ionized, and highly ionized gas are strong and broad and show asymmetrical extensions to $v_{LSR} = -100$ km s^{-1}. The observed profiles are strongly influenced by the effects of Galactic rotation over the large distance to HD 163522. The profiles for interstellar species known to have large scale heights (e.g., Si IV, C IV, and N V) are significantly more affected by Galactic rotation than the profiles for those species more confined to the plane (e.g., H I, Fe II, Mg II, S II, etc.). Simple model calculations are performed to quantitatively understand the characteristics of the observed profiles. Although the sight line passes over the expanding 3 kpc arm at a z distance estimated to be about −0.9 kpc, we find no evidence in the data for absorption at velocities associated with the 3 kpc arm in the underlying disk. The observed absorption line profiles for Al III, Si IV, C IV, and N V are converted into plots of optical depth versus velocity. A comparison of these plots for the weak and strong member of each doublet reveals that the profiles are not strongly influenced by the presence of unresolved saturated absorption and the optical depth profiles can therefore be directly converted into measures of $N(v)$, the column density per km s^{-1}. Integration of the $N(v)$ over the velocity range from −100 to +60 km s^{-1} yields log $N = 13.53$, 13.96, 14.55, and 14.09 for Al III, Si IV, C IV, and N V, respectively. The definite detection of N V with a profile shape that is similar to that of C IV and Si IV favors the origin of these ions in collisionally ionized intermediate temperature gas that may be associated with the nonequilibrium cooling of gas in a Galactic fountain. The observed N V and C IV column densities are compatible with the time dependent ionization calculations published by Edgar and Chevalier in 1986 for a fountain flow rate of 4 $M_{\odot}$ yr^{-1} to each side of the Galactic plane. However, that calculation predicts four times less Si IV than is observed.

Subject headings: galaxies: internal motions — galaxies: The Galaxy — interstellar abundances — stars: individual (HD 163522) — ultraviolet: spectra

I. INTRODUCTION

We have initiated a program to obtain high-quality ultraviolet interstellar absorption line data for very long lines of sight through the interstellar medium of the Galactic disk and low halo. The long paths yield large column densities for such species as Si IV and C IV and permit the reliable detection of absorption by N V, the best interstellar hot gas diagnostic accessible to existing ultraviolet observatories. The emphasis of these studies will be on those lines of sight for which the effects of differential Galactic rotation are substantial. Our goal is to better understand the physical state and kinematics of gas found away from the Galactic plane and, if possible, to use the effects of Galactic rotation to better determine the Galactic distribution of the large number of interstellar species that are accessible to ultraviolet telescopes. In this first paper, which discusses the measurements for one sight line, we emphasize our new analysis techniques and the broader aspects of our research program. In particular, we discuss a technique for converting absorption line profiles into representations of column density per unit velocity, $N(v)$, and indicate how empirical methods can be used to assess the influence of unresolved saturated structure on the column densities. We also discuss how the observed $N(v)$ curves are expected to behave, given assumptions for the scale height of the species being studied and the Galactic rotation curve for matter extending into the halo.

The star we have selected for this first study is HD 163522 which lies in the direction $l = 349.^{\circ}6$ and $b = -9.^{\circ}1$. We show that the UV stellar spectrum of HD 163522 is consistent with its MK classification of B1 Ia and an estimated absolute visual magnitude $M_V \approx -7.0$ (see § III). With $m_V = 8.46$ and $E(B-V) = 0.19$, the implied spectroscopic distance to HD 163522 is about 9.4 kpc placing the star beyond the Galactic center at a distance away from the Galactic plane of approximately −1.5 kpc. The brightness, great distance, and interesting direction of HD 163522 make it well suited for probing the large-scale distribution of interstellar gas in the Galaxy.

The organization of this paper is as follows: in § II we discuss the *IUE* observations and their reductions. In § III we report on the UV stellar data for HD 163522 and establish that the star is very likely a B1 Ia star at a very large distance. In § IV we report on the UV interstellar line spectrum and the

[1] Washburn Observatory, University of Wisconsin–Madison.

[2] Guest Observer with the *International Ultraviolet Explorer Satellite*, sponsored and operated by the National Aeronautics and Space Administration (USA), by the Science and Engineering Research Council (UK), and by the European Space Agency.

[3] Applied Research Corporation.

TABLE 1

HIGH-DISPERSION *IUE* ECHELLE SPECTRA OF HD 163522

Image Number	Exposure Time (minutes)	Position of Star in Aperture	Velocity Shift[a] (km s^{-1})	Comment
		LWP Detector		
11859.....	60	Center	−10	Saturation near $\lambda \approx 2800$ Å
15120.....	40	Center	−10	
		SWP Detector		
22492.....	120	Center	+5	Saturation for $\lambda > 1864$ Å
32072.....	120	10″ offset	−26	
32073.....	150	Center	0	Saturation for $\lambda > 1864$ Å
35645.....	240	Center	0	Saturation for $\lambda > 1800$ Å

[a] The velocity shift applied to each spectrum to bring them into a common heliocentric velocity system is defined by $v_{\rm helio} = v_{\rm obs}$ + velocity shift.

special reduction technique we employ to convert the data into physically meaningful quantities. The emphasis of our study is on the absorption produced by the highly ionized gas. In § V we overview general aspects of the sight line which are relevant to the detailed discussions of the kinematics of the gas in § VI and the physical conditions of the gas in § VII. Our results are summarized in § VIII.

II. OBSERVATIONS

We obtained the *IUE* high-dispersion echelle spectra of HD 163522 listed in Table 1. The spectra cover the far-UV (SWP camera, $\lambda \approx$ 1150–2000 Å) and middle-UV (LWP camera, $\lambda \approx$ 2000–3200 Å) with resolutions of 20–25 km s^{-1}. For information about the *IUE* spacecraft and its spectrographs, see Boggess *et al.* (1978*a*, *b*). The different spectra were obtained with the star at various positions in the large-entrance (10″ × 20″) aperture in order to reduce the effects of the fixed pattern noise in the *IUE* intensified vidicon detectors. The individual spectra were processed with Version 2 of the *IUE* standard spectral extraction routines available at the Goddard Space Flight Center (Turnrose and Thompson 1984).

For our stellar investigation (see § III), plots of flux versus wavelength obtained from the standard processing of individual spectra were produced by combining the derived fluxes from the different echelle orders and averaging the result over 0.25 Å with a Gaussian filter.

For our interstellar investigation (see § IV), we were interested in obtaining spectra with the highest possible signal-to-noise ratio. The different spectra were averaged after determining the velocity shifts required to bring them into a common velocity system. Since spectrum SWP 32073 was obtained with the star centered in the large aperture, we assumed that the normal reduction provided the correct heliocentric velocities for that spectrum. The accuracy of the velocities in individual *IUE* high-resolution spectra has been studied by Thompson, Turnrose, and Bohlin (1982) with the result that the 2 σ uncertainty for spectra properly centered in the large aperture is 4 km s^{-1}. For spectral lines near the edges of the echelle orders, the uncertainty may be somewhat larger. The velocity shifts required to align the other spectra with SWP 32073 were determined with reference to the numerous narrow interstellar lines and are listed in Table 1. A single velocity shift was then applied to each SWP or LWP spectrum. The LWP spectra were registered to the SWP spectra by requiring the middle-UV lines of Fe II to have the same velocity as the Fe II line at 1608.456 Å. In the processing of the individual spectra, the linearized data numbers were corrected for the instrumental background, the echelle blaze function, and the instrumental sensitivity following the standard procedures. For $\lambda < 1300$ Å, an additional background level shift of about 10% was applied with reference to the cores of the highly saturated interstellar lines. To produce an averaged spectrum, the final derived signal (i.e., flux times integration time) for the individual spectra were linearly interpolated into 5 km s^{-1} velocity bins and added.

III. THE STELLAR SPECTRUM

HD 163522 was classified as a normal B1 Ia by Garrison, Hiltner, and Schild (1977), but because of its implied location, 1.5 kpc below the Galactic plane, one might suspect that it is not a normal Population I B supergiant. To investigate this possibility, we conducted a detailed comparison of its UV spectrum with those of B supergiants considered normal by Walborn (1976, Table 5). Figure 1 compares the $\lambda\lambda$1200–1600 spectral regions of HD 163522 to those of the normal supergiants HD 91943 (B0.7 Ia) and HD 148688 (B1 Ia). In the ultraviolet, photospheric and wind lines can be used to determine a star's spectral type.

a) Photospheric Lines

The photospheric silicon spectrum of HD 163522 is indicative of a high luminosity star with a spectral type near B1. As can be seen from Figure 1, the Si II λ1265 and Si III λ1299 lines of HD 163522 are very similar to those of HD 148688 in both demonstrates that the ratio of these two lines is very temperature sensitive, we estimate a spectral type near B1. Massa also shows that the strength of the Si III λ1417 singlet is an excellent luminosity diagnostic. This line in HD 163522 is as strong as the one in HD 148688 which, in turn, is the strongest Si III λ1417 line in Massa's sample. Therefore, the UV photospheric silicon spectrum of HD 163522 indicates that it is a very luminous B1 star.

In addition to the silicon lines, photospheric carbon lines from both C II and C III are present in the UV spectra of early B stars. Wollaert, Lamers, and de Jager (1988) discuss the C III λ1247 line in a few early B stars, and work in progress (Massa 1990) employs both C III λ1247 and C II λ1324. A preliminary

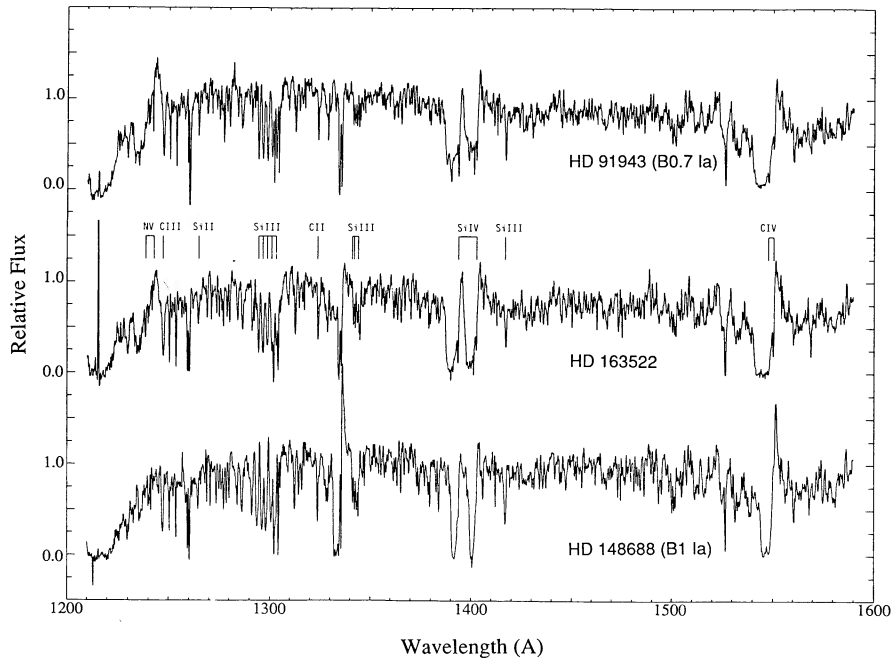

FIG. 1.—Relative flux vs. wavelength in Å based on single high-resolution *IUE* spectra for HD 91943, HD 163522, and HD 148688. The spectra have been smoothed with a 0.25 Å FWHM Gaussian filter. Various stellar lines are identified above the spectrum for HD 163522. HD 91943 and HD 148688 are classified by Walborn (1976) as normal B0.7 Ia and B1 Ia stars, respectively. The UV photospheric and stellar wind features for HD 163522 imply a classification of B1 Ia and hence $M_V = -7.0 \pm 0.5$ mag.

result of Massa's study is that the most useful C II line to use as a luminosity diagnostic is λ1324. The line is very strong in HD 163522 and HD 148688, implying that both of these are very luminous stars with spectral class later than B0.5. The C II λ1760 multiplet is also quite strong in all three stars, but heavy line blanketing in this region makes continuum placement ambiguous and simple quantitative comparisons difficult. Of the C III lines, λ1247 is the most useful. It is very strong in all three stars, implying that they must be very luminous B1 or earlier stars. The C III λ1175 multiplet is not relied upon because it is highly saturated and, more importantly, occurs at a wavelength where the response curve of the *IUE* detector is dropping off rapidly, making uniform exposure across the line difficult and calibration of the detector non-linearity untrustworthy.

Most of the UV photospheric carbon and silicon lines of HD 163522 indicate that it is a very luminous B1 star. One exception is the Si III λ1342 multiplet which is stronger than that of HD 91943 yet weaker than that of HD 148688. It is possible that the relative weakness of this multiplet near B1 makes it an important diagnostic feature, but the multiplet has not been studied in a sufficient number of stars to determine how its strength responds to temperature and luminosity relative to the other Si III lines.

b) Wind Lines

The wind lines are important in several respects. Walborn and Nichols-Bohlin (1987) demonstrate that the UV wind lines of OB supergiants are very sensitive to spectral class, and Walborn and Panek (1985) show that abundance anomalies result in specific patterns of abnormal wind line strengths. In addition, Ebbets and Savage (1982) explain how the terminal velocity of wind lines can be used to uncover suspected subluminous stars. Therefore, the wind lines are not only useful for determining the spectral type of a star, but also for deciding whether the star has a spectroscopic peculiarity which might lead one to suspect that it is not a normal Population I supergiant.

Beginning at the shortest wavelengths, the N V λ1240 wind lines in HD 163522 resemble those in the B0.7 Ia HD 91943, although they are somewhat weaker. The C II λ1335 wind lines in HD 163522 are weak, while they are quite strong in HD 148688 and completely absent in HD 91943. The Si IV λ1400 lines are saturated in all three stars. The Si IV terminal velocity and emission strength in HD 163522 are between those in the B0.7 and B1 supergiants. The C IV λ1550 profile behaves similarly to the Si IV profile. Much of the apparent "square-bottomed" shape of the C IV absorption in HD 163522 is the result of interstellar absorption affecting the low velocity portion of the profile. Although not shown, the Al III λ1860 lines behave very similarly to the C II lines; they are well developed in HD 148688, beginning to develop in HD 163522, and photospheric in HD 91943.

The strengths and terminal velocities of the HD 163522 wind lines are intermediate to those of the B0.7 and the B1 supergiants in every respect. In fact, the line strengths of HD 163522 place the spectral type quite consistently between B0.7 and B1 in Figure 11 of Walborn and Nichols-Bohlin (1987). The fact that the photospheric line strengths in HD 163522 are nearly identical to those of a B1 supergiant while its wind lines are between those of B0.7 and B1 supergiants is not a concern because the strong photospheric silicon and carbon lines are near a plateau of maximum strength at B1, making them less sensitive to spectral class than they may otherwise be.

c) Discussion

We are confident in classifying HD 163522 as a normal B0.7–1 Ia, consistent with the ground-based classification.

Consequently, we can assign an absolute magnitude of $M_V = -7 \pm 0.5$ mag based on Walborn's (1972) spectral type–M_V calibration. With $E(B-V) = 0.19$ and $A_V/E(B-V) = 3.1$, the estimated distance of HD 163522 is $d = 9.4^{+2.4}_{-1.9}$ kpc.

Because of the star's great distance, it is interesting that the spectrum of HD 163522 fits so neatly between those of solar neighborhood supergiants without obvious inconsistencies. The nominal galactocentric distance of HD 163522, R, is 1.8 kpc (assuming $R = 8.5$ kpc for the Sun). The error limits on the distance imply that the star could be as close to the Galactic center as the tangent point [which occurs at $d \cos(b) = 8.4$ kpc for this line of sight which passes within 1.5 kpc of the Galactic center] and no further from it than 3.6 kpc. In either case, the galactocentric radius of HD 163522 is almost certainly less than half that of the Sun. Given this small galactocentric radius, one may have expected noticeable differences in the photospheric and/or wind line strengths relative to solar neighborhood stars as a result of abundance differences due to the galactocentric abundance gradient. However, most of the photospheric lines discussed above are highly saturated near B1 and are not too sensitive to abundance differences.

The radial velocity of HD 163522 is unusual. Its LSR velocity is $+36$ km s^{-1} (Savage and Massa 1987). Employing Clemens's (1985) Galactic rotation law, we see that positive velocities are not expected for the sight line to HD 163522 for distances less than 17 kpc. The expected radial velocity is -136 km s^{-1} (-169, -47), where the velocities in parenthesis result if the star is at the tangent point or at 1.25 times its nominal distance of 9.4 kpc, respectively. The peculiar (expected minus observed) radial velocity of HD 163522 is -172 km s^{-1}. Although large peculiar motions are common for stars found at large distances from the Galactic plane, a peculiar velocity of this magnitude is rare.

IV. THE INTERSTELLAR SPECTRUM

Selected interstellar absorption lines for HD 163522 are illustrated in Figure 2 where the observed intensity is plotted against LSR velocity. In the direction of HD 163522, $v_{LSR} = v_{helio} + 5.5$ km s^{-1}. The lines illustrated in Figure 2 are listed in Table 2 where we give wavelength, f-value, and comments about the observed absorption. To permit a comparison of ultraviolet absorption and H I 21 cm emission we also illustrate in Figure 2c the 21 cm emission profile from Danly *et al.* (1990) obtained with the 140 foot (42.7 m) NRAO telescope at Green Bank, West Virginia. The 21 cm profile illustrated has not been corrected for the effects of antenna side lobe contamination.

The blending of stellar and interstellar lines is particularly troublesome when studying an object whose interstellar lines are as wide as those of HD 163522. The Si III 1294.54 Å line (illustrated at the top of Fig. 2d) is purely photospheric and can be used to estimate the rotational and radial velocities of HD 163522. Using this line, we estimate $v \sin i \approx 50$ km s^{-1} and v_r(LSR) $\approx +36$ km s^{-1}. The relatively small $v \sin i$ creates serious blending problems for measuring the interstellar absorption by ions which also produce strong photospheric absorption. Fortunately, for the lines of the highly ionized species of abundant elements such as Si IV $\lambda\lambda$1393 and 1402 and C IV λ1550, the interstellar absorption occurs against the relatively smoothly rising continuum provided by the very strong stellar wind P Cygni profiles (see Figs. 1 and 2). Because

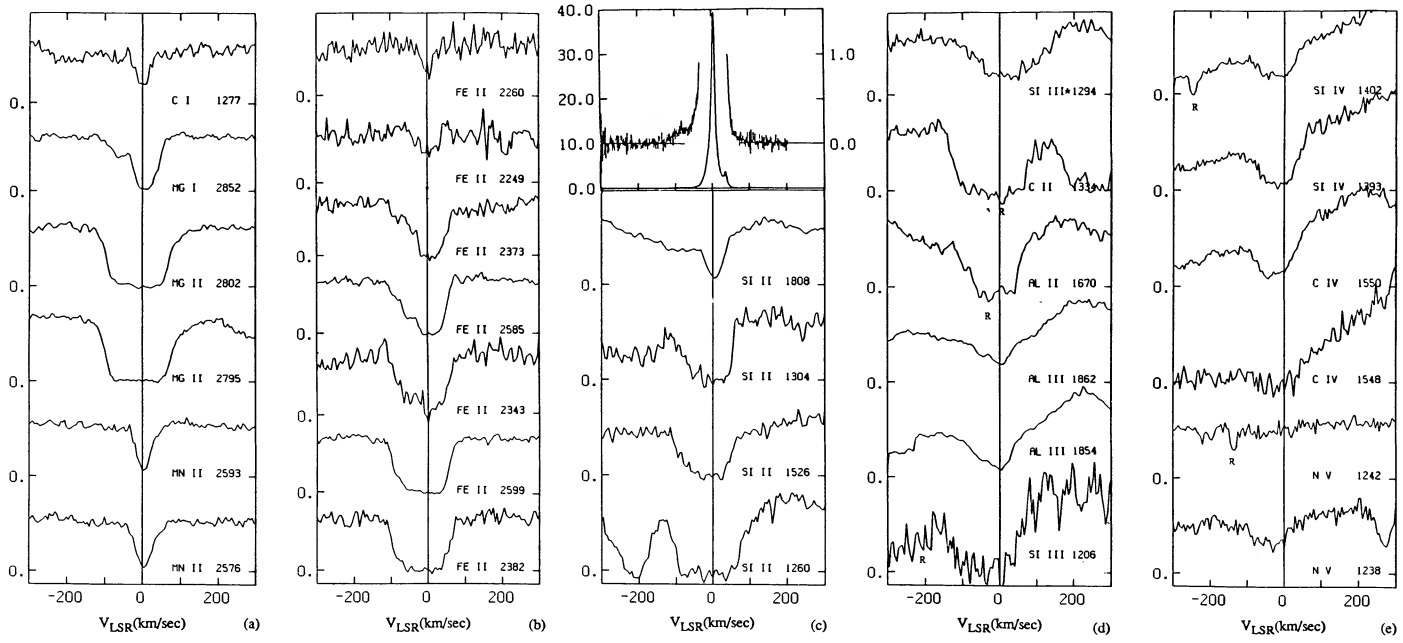

FIG. 2.—High-resolution interstellar line profiles for HD 163522 for the ions listed in Table 2. The zero level of flux is indicated by the tick marks on the vertical axis of each panel. The flux is plotted against LSR velocity via the conversion $v_{LSR} = v_{helio} + 5.5$ km s^{-1}. The profiles shown are averages of three or four SWP spectra or two LWP spectra as listed in Table 1. R indicates the location of a detector reseau. In a number of cases, more than one absorbing species lies in each velocity region as indicated in the comments of Table 2. The Si III λ1294 line is a stellar photospheric feature which is plotted to illustrate the possible effects of stellar line blending. For the important lines of Si IV, C IV, and N V the interstellar absorption is viewed against the strong and relatively smooth stellar P Cygni lines. In the case of Al III, stellar photospheric blending is a source of uncertainty in producing reliable absorption line profiles and optical depth plots. The H I 21 cm emission profile shown in (c) with two scales of antenna temperature plotted vs. velocity is from Danly *et al.* 1990.

TABLE 2

ABSORPTION LINES ILLUSTRATED IN FIGURE 2

Ion	f[a]	Wavelength[b]	Echelle Order	Comment
C I	0.156	1277.245	108	
Mg I	1.77	2852.127	81	
Mg II	0.295	2802.704	82	
	0.592	2795.528	83	
Mn II	0.223	2593.731	89	
	0.288	2576.107	90	
Fe II	0.0028[c]	2260.080	102	
	0.0074[d]	2249.180	103	
	0.0395	2373.733	97	
	0.0573	2585.876	89	
	0.108	2343.495	99	
	0.203	2599.395	89	
	0.328	2382.034	97	
H I	...	21 cm	...	This 21 cm emission profile is from Danly *et al.* 1990
Si II	0.0041[e]	1808.003	76	
	0.100[e]	1304.369	106	
	0.116[e]	1526.719	90	
	0.959	1260.418	109	S II λ1259.520 appears at $v = -214$ km s^{-1}
Si III	...	1294.54	106	This line from an excited level is a stellar photospheric feature
C II	0.118	1334.532	103	C II* λ1335.70 appears at $v = +263$ km s^{-1}
Al II	1.88	1670.786	83	
Al III	0.268	1862.795	74	Stellar blending causes uncertain continuum
	0.539	1854.720	74	Stellar blending causes uncertain continuum
Si II	1.66	1206.510	114	Low signal-to-noise ratio
Si IV	0.262	1402.769	98	
	0.528	1393.755	99	
C IV	0.097	1550.774	89	
	0.194	1548.202	89	Very low signal-to-noise ratio because of the deep P Cygni C IV
N V	0.0757	1242.804	111	
	0.152	1238.821	111	Mg II λ1239.925 appears at $v = +267$ km s^{-1}

[a] f-values are from Morton and Smith 1973 except as noted.
[b] λ's are in vacuum for $\lambda < 2000$ and in air for $\lambda > 2000$.
[c] f value from Shull, van Steenberg, and Seab 1983.
[d] f value from Kurucz and Peytremann 1975.
[e] f value from Luo, Pradhan, and Shull 1988.

the interstellar C IV λ1548 line lies near the bottom of the P Cygni absorption, the background flux is too small for reliable measurements to be made with the existing data.

Note the following characteristics of the interstellar line spectrum of HD 163522. The high ionization lines of C IV and Si IV are strong and broad with absorption at half-intensity extending from about $+20$ km s^{-1} to -80 km s^{-1}. The stronger N V line, λ1238, is definitely detected and exhibits half intensity absorption extending from about $+10$ to -90 km s^{-1}. The weaker N V line, λ1242, is only marginally detected. Although stellar blending is a source of confusion, interstellar Al III is detected through its doublet near 1860 Å and exhibits less absorption at the highest negative velocities compared to Si IV or C IV. The lower ionization lines illustrated in Figure 2 span a very large range of f-value and therefore permit us to study the low ionization absorption in both high and very low column density limits. The weak Fe II and Si II lines detect only high column density local gas near $v \approx 0$ km s^{-1}, while the strongest Fe II and Si II lines are completely saturated from $+30$ km s^{-1} to -100 km s^{-1}.

a) *The Lines of* N V, C IV, Si IV, *and* Al III

For the lines produced by the moderately and highly ionized gas toward HD 163522 (e.g., N V, C IV, Si IV, and Al III), we have produced log plots of *apparent* optical depth, $\tau(v)$, as a function of velocity according to the relation

$$\tau(v) = \ln [I_c(v)/I_{obs}(v)] , \quad (1)$$

where $I_c(v)$ is the estimated intensity in the continuum and $I_{obs}(v)$ is the observed intensity in the absorption line as a function of velocity. The $\tau(v)$ defined here correctly depicts an instrumentally smoothed optical depth only under the condition that $\tau(v) \ll 1$ or if the velocity structure of the observed line is fully resolved by the instrument. If the *apparent* $\tau(v)$'s are indeed valid representations of the true $\tau(v)$'s, they relate to the column density per unit velocity interval through the relation

$$\log [N(v)] = \log \tau(v) - \log (f\lambda) + 14.576 \text{ [atoms cm}^{-2} \text{ (km s}^{-1})^{-1}] , \quad (2)$$

where the wavelength, λ, is in Å. An empirical technique for assessing the amount of unresolved line saturation is to compare the apparent optical depth profiles for different absorption lines due to the same ion but differing in values of the product $f\lambda$. If the derived run of $N(v)$ with v is the same for the two or more lines differing in $f\lambda$, we can be reasonably sure that the derived $N(v)$ curves are not significantly affected by unresolved saturated structure in the line. The reader may wish to refer to Savage *et al.* (1989) for an application of the techniques discussed here to the UV interstellar data for the sight line to SN 1987A.

A continuum is found for each line by fitting a polynomial (order < 5) to regions on either side of the line. These regions were selected to exclude stellar features, cosmic-ray hits, and other obvious contamination. The continuum fit error, σ_c, is taken to be the rms deviation in the data about the derived continuum. We assume that the points used in the continuum fitting procedure are statistically independent, and we assume that the error due to continuum placement is equivalent to raising or lowering the entire continuum by the amount σ_c. This technique provides a generous estimate of the errors associated with continuum placement and continuum curvature. A comparison of the spectrum away from the absorption line centers and near the cores of the lines of the highly ionized species reveals that the statistical fluctuations in the two regions are approximately equivalent. These fluctuations are likely dominated by fixed pattern noise. We therefore estimate the statistical noise fluctuations, σ_s, to be the same as the error in the continuum, σ_c, and add in quadrature the continuum placement error and the statistical error to arrive at a total error.

Plots of the logarithm of the *apparent* optical depth, $\log \tau(v)$, for lines of N V, C IV, Si IV, and Al III are illustrated in Figure 3 as solid lines. When the value of $\tau(v)$ is small and therefore unreliable, the inferred values of $\tau(v)$ are replaced by plus symbols. The dots above and below each line or plus symbol indicate our assessment of the uncertainty in the apparent $\tau(v)$ which is introduced by the uncertainty associated with the error in the continuum placement and with statistical errors. Note that for the lines of N V λ1238, C IV λ1550, and Si IV $\lambda\lambda$1393 and 1402, the continuum is well determined and the derived $\tau(v)$'s are quite reliable. For Al III, stellar blending introduces a substantial error in the derivation of $\tau(v)$ for the line at λ1854 while the continuum for the line at λ1862 is considerably better defined.

Figure 4 compares the $\tau(v)$'s for the Si IV and Al III doublets. The $\tau(v)$ for the weaker component is multiplied by 2 to compensate for the difference in oscillator strengths. The apparent $\tau(v)$ for the strong component and $2\tau(v)$ for the weaker one have very similar shapes for Si IV and similar shapes for Al III (given the continuum uncertainty associated with the stronger Al III line at λ1854). This implies that the apparent optical depths of both ions are indeed valid representations of the true optical depths, degraded in resolution by the 20–25 km s^{-1} instrumental smearing of *IUE*. Therefore, the apparent optical depths most likely do not contain *saturated* unresolved structure and can be reliably converted into $N(v)$, the column density per unit velocity, via equation (2) and the f-values listed in Table 2.

For C IV and N V we have provided $\tau(v)$ plots only for the more reliable measures of the lines near λ1550 and λ1238, respectively. Both lines have shapes roughly similar to Si IV and apparent optical depths between those for the two Si IV lines. This result leads us to conclude that the apparent $\tau(v)$'s for C IV and N V are probably also unaffected by unresolved saturated structure.

Having established that line saturation is not seriously influencing the $\tau(v)$'s illustrated in Figure 4, we employ equation (2) to obtain estimates for the line-of-sight column densities of each ion from $N(\text{atoms cm}^{-2}) = \int N(v)dv$. The results are given in Table 3 for the various lines and the indicated velocity ranges. We also list upper and lower 1 σ limits for $N(v)$ based on estimates of the errors discussed above. Table 3 also contains the measured line equivalent widths and their $\pm 1\ \sigma$ errors. In those cases where both components of the various doublets have been measured, an independent *but less reliable* method for computing the column density is through standard curve-of-growth fitting assuming a simple form for the line broadening. In the case of a simple single-component Doppler-broadened curve of growth characterized by the Doppler spread parameter b(km s^{-1}), we obtain $\log N(\text{Si IV}) = 13.8 \pm 0.13(1\ \sigma)$ with $b = 70$ km s^{-1} and $\log N(\text{Al III}) = 13.5 \pm 0.3(1\ \sigma)$ with $b = 62$ km s^{-1}. The large values of b are consistent with the large observed widths of the lines. However, the observed asymmetric shapes of the lines clearly indicate that a simple curve of growth is a poor representation of the true velocity distribution for the sight line to HD 163522. The reason the simple curve of growth gives values of $\log N$ reasonably close to those in Table 3 is because the lines of Si IV and Al III are relatively weak and hence the inferred column density is relatively independent of the detailed nature of the broadening.

b) H I 21 *Centimeter Emission Profile and Absorption by* Fe II

For comparison with the $N(v)$ plots for the highly ionized gas, a plot of $N(v)_{\text{H I}}$ from the H I 21 cm data of Danly *et al.*

TABLE 3

COLUMN DENSITIES TOWARD HD 163522[a]

Ion	λ(Å)	$W_\lambda \pm 1\ \sigma$ (mÅ)	Velocity Integration Range v_- (km s^{-1})	Velocity Integration Range v_+ (km s^{-1})	$\log N$ $(-1\ \sigma)$	$\log N_{\text{best}}$	$\log N$ $(+1\ \sigma)$
Al III	1854.720	385 ± 32	−110	+60	13.46	13.55	13.62
	1862.795	213 ± 33	−110	+60	13.38	13.51	13.61
Si IV	1393.755	473 ± 32	−110	+60	13.81	14.02	14.16
	1402.769	267 ± 52	−110	+60	13.70	13.91	14.05
C IV	1550.774	447 ± 33	−110	+60	14.44	14.55	14.64
N V	1238.820	200 ± 35	−110	+60	13.91	14.09	14.21
	1242.804	74: ± 45	−110	+60	13.03:	13.89:	14.16:

[a] Best values and 1 σ upper and lower limits to column densities for each high ionization absorption line are listed for the various ions. These estimates are based on a direct integration of the optical depth profiles shown in Fig. 3. The $\pm 1\ \sigma$ upper and lower limits to N include the uncertainty associated with the statistical uncertainty in the measurements and the uncertainty associated with the continuum placement.

(1990) is shown in Figures 5*a* and 5*d*. We assume the 21 cm emission is optically thin and utilize the conversion $N(v)_{\rm H\,I} = 1.82 \times 10^{18}\ T_b(v)$, where $T_b(v)$ is the observed brightness temperature (see Fig. 2*c*) in K. The derived $N(v)_{\rm H\,I}$ profile is plotted at the observed resolution (1 km s^{-1}) in Figure 5*a* and convolved with *IUE* instrumental spread function (taken to be a Gaussian with FWHM = 20 km s^{-1}) in Figure 5*d*. A comparison of Figure 5*d* for H I and Figure 3 for N V, C IV, Si IV, and Al III reveals that the profiles of the highly ionized gas are substantially broader and show greater extension to negative velocities than the H I profile. Some of the differences may arise because the 21 cm emission is averaged over a 20′ (FWHM) beam, while the ultraviolet data sample a solid angle equal to the angular size of the star. Differences could also be

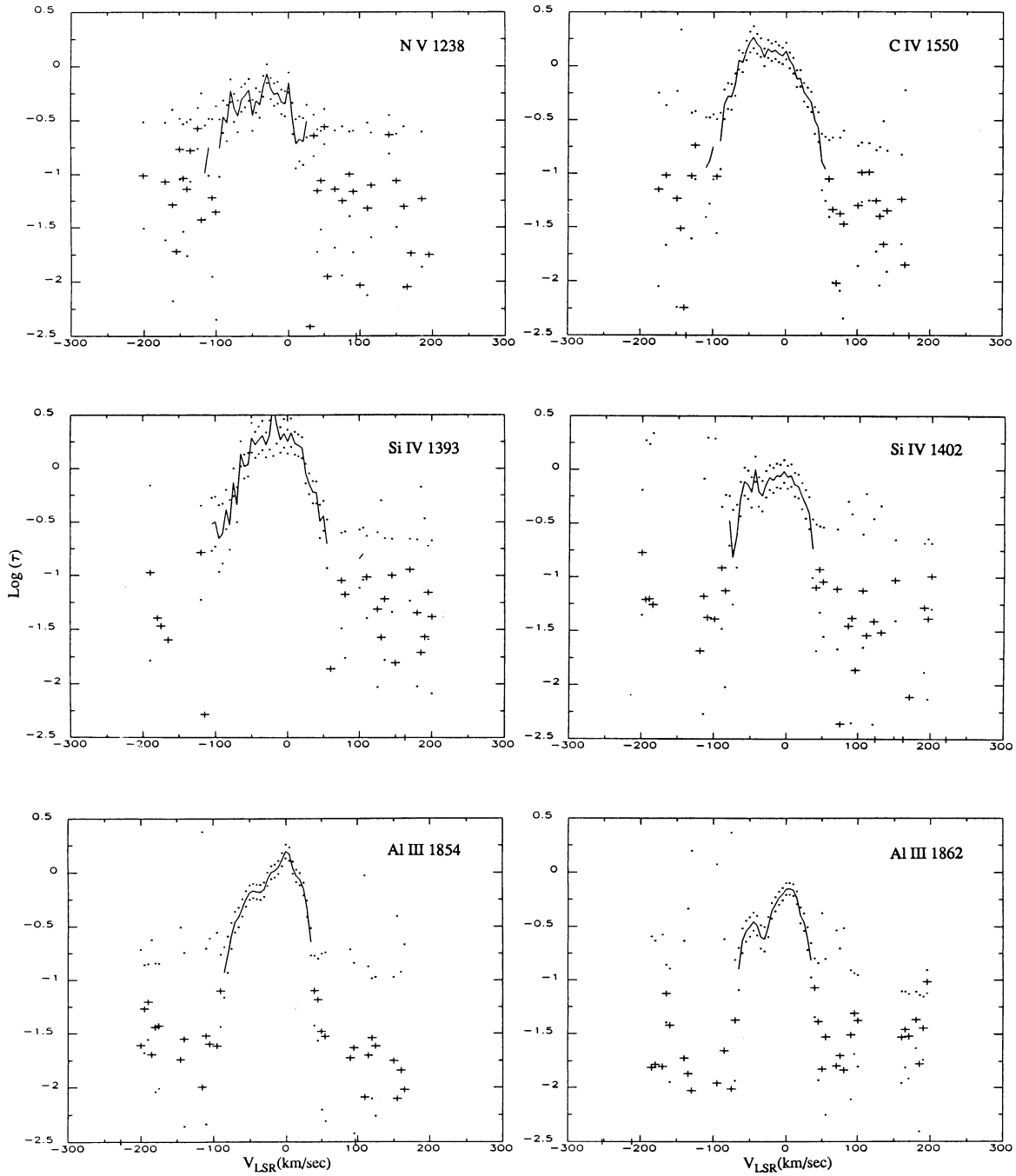

FIG. 3.—Logarithmic plots of *apparent* optical depth, $\tau(v)$, vs. LSR velocity for various lines of the ions N V, C IV, Si IV, and Al III are illustrated with the solid lines. The poorly determined optical depth plots for C IV λ1548 and N V λ1242 have not been plotted. The apparent optical depth, $\tau(v)$, is defined in eq. (1) in the text. When the values of $\tau(v)$ are small and therefore unreliable, the inferred values are replaced by the plus symbols. The dots above and below each solid line or plus symbol represent our best estimate of the 1 σ errors associated with the combined effects of statistical noise and the uncertainty associated with the positioning of the continuum level. If the apparent $\tau(v)$'s are indeed valid representations of the true $\tau(v)$'s, then equation (2) can be used to relate $\tau(v)$ and the column density of the species per unit velocity interval, $N(v)$.

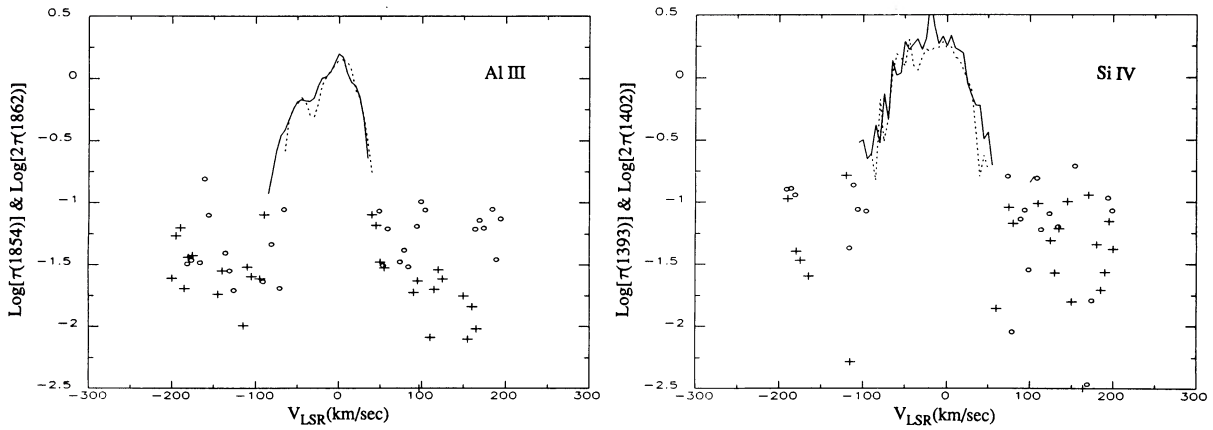

FIG. 4.—Logarithmic plots of apparent optical depth, $\tau(v)$, vs. LSR velocity for the weak (*dashed line*) and strong (*solid line*) components of the Al III and Si IV doublets. The $\tau(v)$ for the weak lines are multiplied by a factor of 2 to account for the difference in oscillator strengths between the strong and weak components. When $\tau(v)$ is very small and unreliable, it is plotted with the open circle and plus symbols for the weak and strong components, respectively. The agreement between the profiles in each doublet suggests that the lines do not contain unresolved *saturated* structure and that eq. (2) can be used to relate $\tau(v)$ and $N(v)$. The disagreement on the negative velocity side of the Al III profiles is probably due to continuum placement ambiguity caused by stellar blending in the stronger line (see Fig. 2*d*).

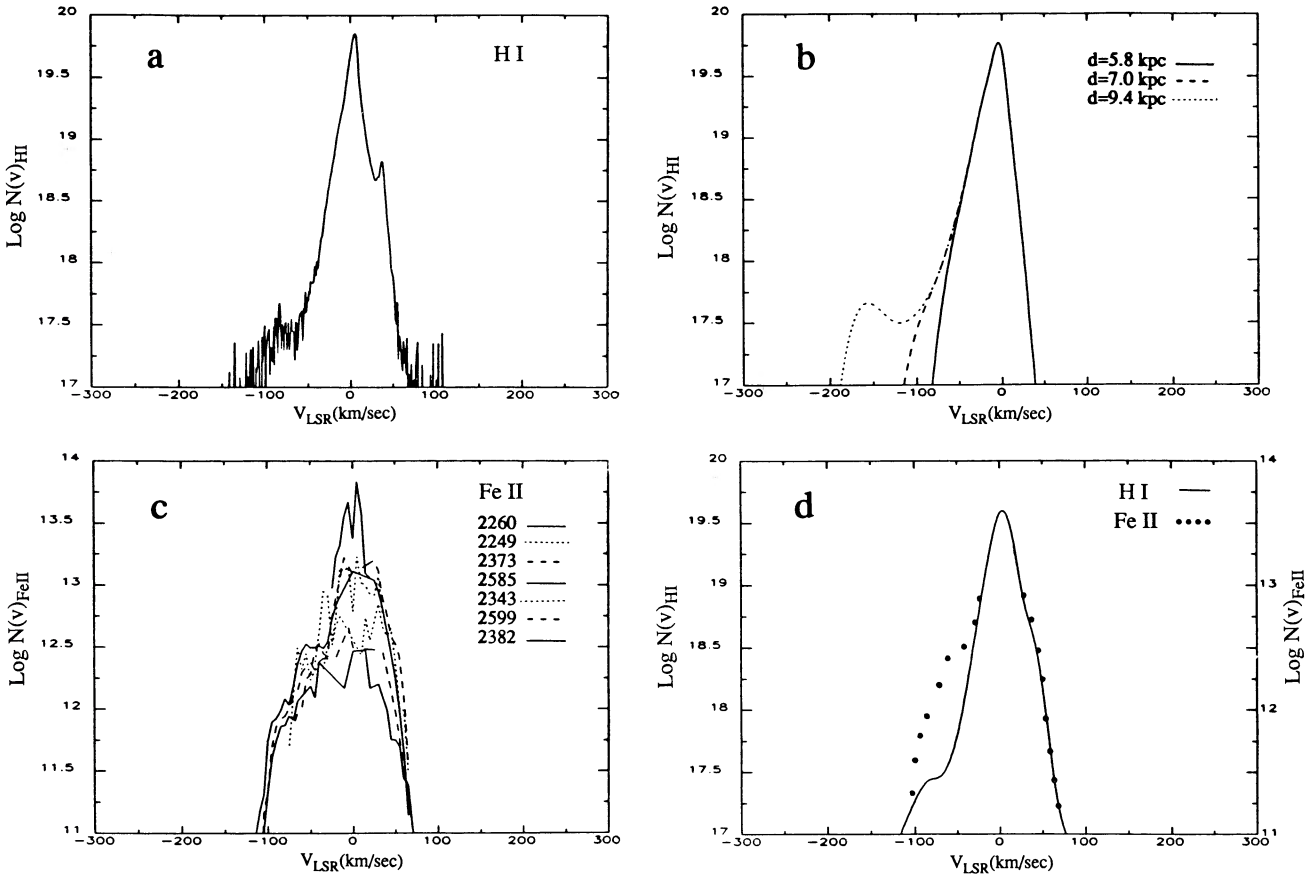

FIG. 5.—(*a*) Logarithmic plot of H I column density vs. LSR velocity derived from the 21 cm profile shown in Fig. 2*c*. The emission profile was converted from brightness temperature into column density via the equation $N_{\rm H\,I}(v) = 1.82 \times 10^{18} T_b(v)$ which assumes that the H I is optically thin. The measurements are plotted at the full 1 km s^{-1} resolution of the original data. (*b*) Logarithmic plot of calculated H I column density per unit velocity, $N(v)_{\rm H\,I}$, vs. LSR velocity assuming corotation of disk and halo gas, and using the model parameters for H I from Lockman (1984) described in § VI*a*. The model calculations are presented for three assumed distances over which H I might exist: d = 5.8 kpc (*solid*), 7.0 kpc (*long dashes*), and 9.4 kpc (*short dashes*). (*c*) Logarithmic plot of column density vs. LSR velocity for the seven Fe II lines listed in Table 2. The apparent optical depths resulting from the profiles in Fig. 2*b* were converted to column densities via eq. (2) in the text using the f-values from Table 2. The profiles are plotted alternately as solid, long dashed, and short dashed lines. The stronger lines are clearly saturated in their cores and provide information only out in the wings of the profiles. (*d*) Logarithmic plot of column density vs. LSR velocity for the H I profile shown in (*a*) smoothed to *IUE* resolution with a Gaussian having a FWHM of 20 km s^{-1} (*solid line*) and for the "best" profile for Fe II (*dotted line*) inferred from Fig. 5*c*. The Fe II column density axis is labeled on the right-hand side of the plot. Note that for $v < -40$ km s^{-1} the value of $N(v)_{\rm Fe\,II}/N(v)_{\rm H\,I}$ is much larger than for $v > -40$ km s^{-1}.

produced if some of the emitting H I lies beyond the star. However, a comparison of the total H I column density derived from the 21 cm emission data [log N(H I) = 21.14 for optically thin emission; Danly *et al.* 1990] and from the ultraviolet Lyman-α absorption [log N(H I) = 21.04 $\pm$ 0.1; Savage and Massa 1987] suggests that most of the emitting H I lies in front of the star.

A few weakly ionized or neutral species have several absorption lines with different oscillator strengths in the *IUE* wavelength range. For these ions, it is possible to construct a composite $N(v)$ profile by combining the results from all the lines which have reliable data over some velocity range. In these cases, the weakest absorption lines provide information about $N(v)$ near $v = 0$ km s^{-1}, where $N(v)$ is largest, while the strongest lines only provide information about $N(v)$ at high velocities, where $N(v)$ is relatively small. The degree of saturation can be inferred by comparing the overlapping regions of lines with different strengths. In velocity regions where the profiles agree for lines with different f-values, we can be reasonably confident that the derived $N(v)$ is relatively unaffected by unresolved saturated components. Figure 5*c* displays the individual $N(v)_{\rm Fe\ II}$ profiles inferred from the Fe II lines $\lambda\lambda$2260, 2249, 2373, 2585, 2343, 2599, and 2382. The effects of saturation in the strongest lines are readily apparent at small velocities where the inferred values of $N(v)_{\rm Fe\ II}$ are much smaller than those obtained for the weaker lines. Note how the degree of saturation increases with $f\lambda$. From the data in Figure 5*c*, a composite profile was constructed based on our estimate of the run of $N(v)_{\rm Fe\ II}$ with v as seen with the *IUE* instrumental smearing of 20 km s^{-1}. The composite curve generally follows the upper envelope of overlapping measurements for the individual $N(v)_{\rm Fe\ II}$ curves in Figure 5*c*. The composite Fe II profile is plotted in Figure 5*d* which also shows the $N(v)$ curve for H I from Figure 5*a* degraded in resolution to match the resolution of *IUE*. The composite $N(v)_{\rm Fe\ II}$ profile is probably reliable over the velocity ranges -100 to -30 km s^{-1} and $+30$ to $+70$ km s^{-1}. Between -30 and $+30$ km s^{-1}, unresolved saturated components may be lowering the observed value of $N(v)_{\rm Fe\ II}$ for the λ2260 line, and we therefore omit the Fe II measurements in this region of Figure 5*d*.

V. PROPERTIES OF THE SIGHT LINE TO HD 163522

Much of the discussion in this paper depends upon the parameters we employ to describe the Galaxy. We use the notation R, z, and d for galactocentric distance, distance away from the midplane, and line-of-sight distance, respectively. We adopt Clemens's (1985) rotation curve with a linear speed and galactocentric distance for the Sun of 220 km s^{-1} and 8.5 kpc, respectively.

The 9.4 kpc sightline to HD 163522 passes through many different regions of the interstellar medium. These probably include the local neutral disk gas, the neutral intercloud medium, the ionized intercloud medium, and the neutral and ionized gas of the Galactic halo. Because the line of sight passes so near the Galactic center, large velocity shifts should result from differential Galactic rotation. The resultant absorption line profiles clearly show such effects through the pronounced asymmetric extension of the absorption to large negative LSR velocities. The line of sight also passes over several distinct and well-studied features in the Galactic plane, including the Sagittarius arm and the 3 kpc arm.

The well-defined Sagittarius arm extends from $l = 274°$ to 32°, is located approximately 1.5 kpc from the Sun, and contains H II regions with LSR velocities of -5 to -15 km s^{-1} (Courtes 1972). The sight line passes about 250 pc below the arm. From Ca II absorption line measurements, Rickard (1974) has found peculiar velocities in the arm of approximately -30 to -45 km s^{-1} in the longitude range from 340° to 0°.

In the direction $l = 350°$, the peak 21 cm emission shifts from near -5 km s^{-1} in the plane to slightly positive velocities at larger $|b|$ (see Burton 1985). This shift is probably related to a relatively nearby H I cloud in this direction whose mean velocity is $+5$ km s^{-1} and which dominates the emission at higher latitudes. The extent of this local cold H I cloud is discussed by Rickard (1974, his group E feature). It is seen in Ca II absorption at small positive velocities ($+4$ to 7 km s^{-1}) throughout the region $l \sim 345°$ to 25° and at all of the latitudes covered by stars in Rickard's sample. This includes a few objects with $b \sim -6\overset{\circ}{.}5$ near $l = 350°$ and a few with $b < -9°$ at positive longitudes. Rickard places the cloud at about 800 pc, implying that the line of sight toward HD 163522 intercepts the cloud at $z \sim -125$ pc. The maximum of the H I emission toward HD 163522 appears near 6 km s^{-1} (see Fig. 2*c*). Absorption by material in this cloud and in the Sagittarius arm will probably affect at least the low ionization state absorption line profiles in the spectrum of HD 163522. Note that the Danly *et al.* (1990) 21 cm emission profile also reveals a weaker H I feature near 37 km s^{-1}. Although the $+37$ km s^{-1} feature is of unknown distance, the absorption-line data for certain species found in the neutral gas indicates that a component lies near $+40$ km s^{-1} which appears to constrain the emitting gas to lie between the Sun and HD 163522.

The 3 kpc arm is another well-studied feature of the Galactic plane. It can be followed in longitude from 338° to 6° and has a mean latitude of $+0\overset{\circ}{.}1$ (Oort 1977). It has a radial velocity of -53 km s^{-1} at $l = 0°$ and is located at a galactocentric distance of about 3.2 kpc. H I maps from Burton (1985, map B183) indicate that H I emission associated with the arm peaks near -110 km s^{-1} at $l = 350°$. These maps also indicate that the H I emission is strong from about -90 to -130 km s^{-1} and is confined to $|b| < 5°$ at these velocities. At lower velocities (-50 to -80 km s^{-1}), the H I emission extends over the range $|b| < 8°$–10°. The H I profile in Figure 2*c* exhibits a weak ledge of emission extending from about -80 to -100 km s^{-1}. It is not clear whether the emission at these velocities is associated with the 3 kpc arm or with high-z neutral gas at other distances. If the estimated distances to the 3 kpc arm and HD 163522 are correct, then the sight line passes over the arm at $z \approx -0.9$ kpc. We note that none of the observed profiles of either the high- or low-ionization species show significant absorption at velocities associated with the 3 kpc arm in the disk (near -110 km s^{-1}).

The central direction of the Galaxy from $l \approx 330°$ to 20° is a strong emitter of M_1 band (0.44–1.1 keV) X-rays (Nousek *et al.* 1982; McCammon *et al.* 1983). While much of this emission may be associated with the nearby region that causes the North Polar Spur feature (seen in soft X-ray, 21 cm, and radio continuum surveys), it is quite possible that substantial emission is also associated with hot gas (log $T = 6.5$) situated in the central region of the Galaxy. An absorption optical depth of one for M_1 band X-rays occurs for N(H I) = 1.1×10^{21} atoms cm^{-2}. Since the measured value of N(H I) in front of HD 163522 from Lyman-α absorption is also 1.1×10^{21} atoms cm^{-2} (Savage and Massa 1987), it appears that the X-ray absorption optical depth in the direction of HD 163522 is small enough to permit X-rays emitted from hot gas in the

central region of the Galaxy to reach the Sun. It is interesting that the zone of enhanced X-ray emission from the Galactic central regions has the same approximate extent in longitude ($\approx \pm 25°$) as the 3 kpc arm. Perhaps the 3 kpc arm and the region of enhanced X-ray emission have a common origin. The process that created the arm may also be responsible for the absence of high-altitude H I in the central region of the Galaxy, i.e., for galactocentric distances $R < 3$–4 kpc (Lockman 1984).

VI. KINEMATICS OF THE GAS TOWARD HD 163522

The shape of an interstellar absorption profile obtained for a given sight line depends upon both the spatial and kinematical distributions of gas. In this section, we concentrate upon the kinematical influences and their effect upon the *shape* of the absorption line, or equivalently, the form of the $\tau(v)$ and $N(v)$ curves derived in § IV. In § VI*a*, we present the model for the absorbing gas layer and in § VI*b* describe how varying the different physical parameters influences the form of $\tau(v)$ or $N(v)$. In § VI*c*, we compare the observed profiles for HD 163522 to the model calculations and discuss the implications in § VI*d*. Future papers will consider other sight lines.

a) The Model Absorbing Gas Layer

We have constructed a simple model for the absorbing gaseous layer in order to interpret the observed characteristics of curves of $\tau(v)$ or $N(v)$. Given expressions for the Galactic rotation law, the velocity dispersion of an ion, and the ionic density, as functions of galactocentric radius, R, and Galactic altitude, $|z|$, a computer program divides the path into small (50 pc) intervals, keeping track of the maximum and minimum velocities, velocity dispersion, and the mean density encountered in each interval. This information is then converted into column densities as a function of velocity for each interval. Finally, the contributions of each interval to each velocity point in a specified grid are summed to produce the final result. Such a model treats the gas between the program star and the Sun as a smooth medium whose properties vary slowly with distance.

Clearly, the choice of the Galactic rotation law, velocity dispersion, and density distribution along the line of sight influence the shape of the resulting absorption line. Since we cannot hope to determine all of these factors by examining a single line of sight, we seek to specify as many of the parameters as possible *a priori*. For the HD 163522 sight line, we adopt the Galactic rotation law derived by Clemens (1985). Since departure from corotation can have a major effect on the profiles, we must also define how the rotation curve behaves perpendicular to the plane. A departure from corotation above the disk is modeled by multiplying the rotation curve for the plane by a function of $|z|, f(|z|). f(|z|) = 1$ in the plane and can be allowed to decrease with increasing $|z|$.

We must also specify the functional form of the density distribution of the gas with respect to R and $|z|$. We rely on Lockman's (1984) results which imply that the midplane density and z-dependence of the gas, at least for the extended components of H I, are independent of R for $3 < R < 8.5$ kpc. Since the sight line for HD 163522 passes within 1.5 kpc of the Galactic center, it is necessary to guess how the density of the gas behaves between $R = 1.5$ and 3 kpc. To specify the functional form of the $|z|$ distribution of the gas, we employ the distributions obtained by Lockman (1984) and Savage and Massa (1987) as guides for the neutral and highly ionized atoms, respectively. The H I distribution obtained by Lockman is a sum of two Gaussians and an exponential. The analysis of Savage and Massa provided only estimates of the scale heights for simple exponential distributions. Finally, we assume that the gas velocity dispersions, which are a result of cloud-to-cloud motions and thermal Doppler motions, are independent of R and $|z|$.

b) Factors Influencing the Shape of the Observed Profiles

Because so many parameters can affect the profile shapes, and because none are exactly known, it is valuable to examine how varying the model parameters about their adopted values affect the computed profiles. The solid line in Figure 6 shows how the radial velocity of the absorbing gas along the line of sight to HD 163522 behaves under the assumption that the Galactic halo and disk corotate. This function, together with one for the density of the gas along the line of sight, determines the overall shape of the observed $\tau(v)$ or $N(v)$ profile. The main effect of the local velocity dispersion is to smooth the profiles in velocity space.

The effect of varying the scale height of an exponentially distributed gas is displayed in Figure 7*a* for scale heights, $H = 0.5$, 1.0, and 3.0 kpc, which span the range of scale height estimates for the low and high ions. The relative contribution of the high-velocity gas to the profile increases dramatically with increasing scale height, as might be expected from Figure 6. The velocity dispersion of the absorbing gas, σ, was held fixed at 10 km s^{-1} for each case. Increasing or decreasing the velocity dispersion of the gas produces a broadening or narrowing of the derived profiles. Note that none of the curves illustrated in Figures 7*a*, 7*b*, and 7*c* have been convolved with the *IUE* spread function.

The effects produced by either varying the distance to the star or by allowing for a reduction in the gas density for $R < 3$ kpc (as might be expected from Lockman's 21 cm emission-line results, at least for the neutral gas) are related; cutting off the contribution by gas inside 3 kpc is essentially the same as moving the position of HD 163522 to $R = 3$ kpc, which occurs at a line-of-sight distance of 5.8 kpc. Model results for stellar

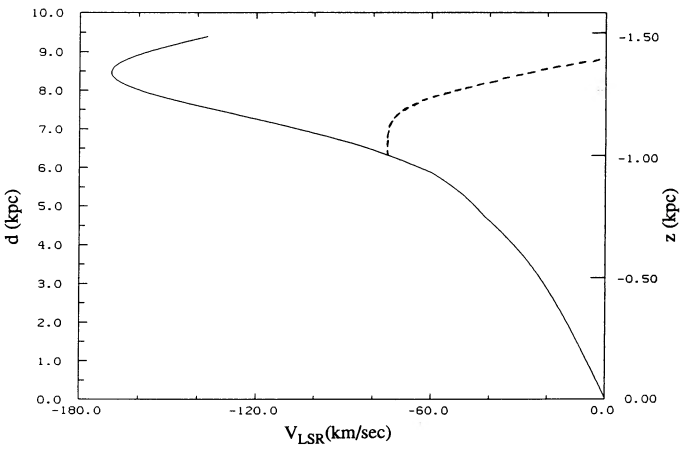

FIG. 6.—LSR radial velocity for gas to HD 163522 as a function of line-of-sight distance, d (kpc), and distance away from the Galactic plane, z (kpc). The solid curve assumes pure corotation of disk and high-z gas using the Galactic rotation curve of Clemens (1985). The dashed curve illustrates a case where deviations from corotation, as defined by $f(|z|)$ (see § VI), set in at $z = -1$ kpc and linearly decrease to zero at $z = -1.5$ kpc, remaining zero thereafter.

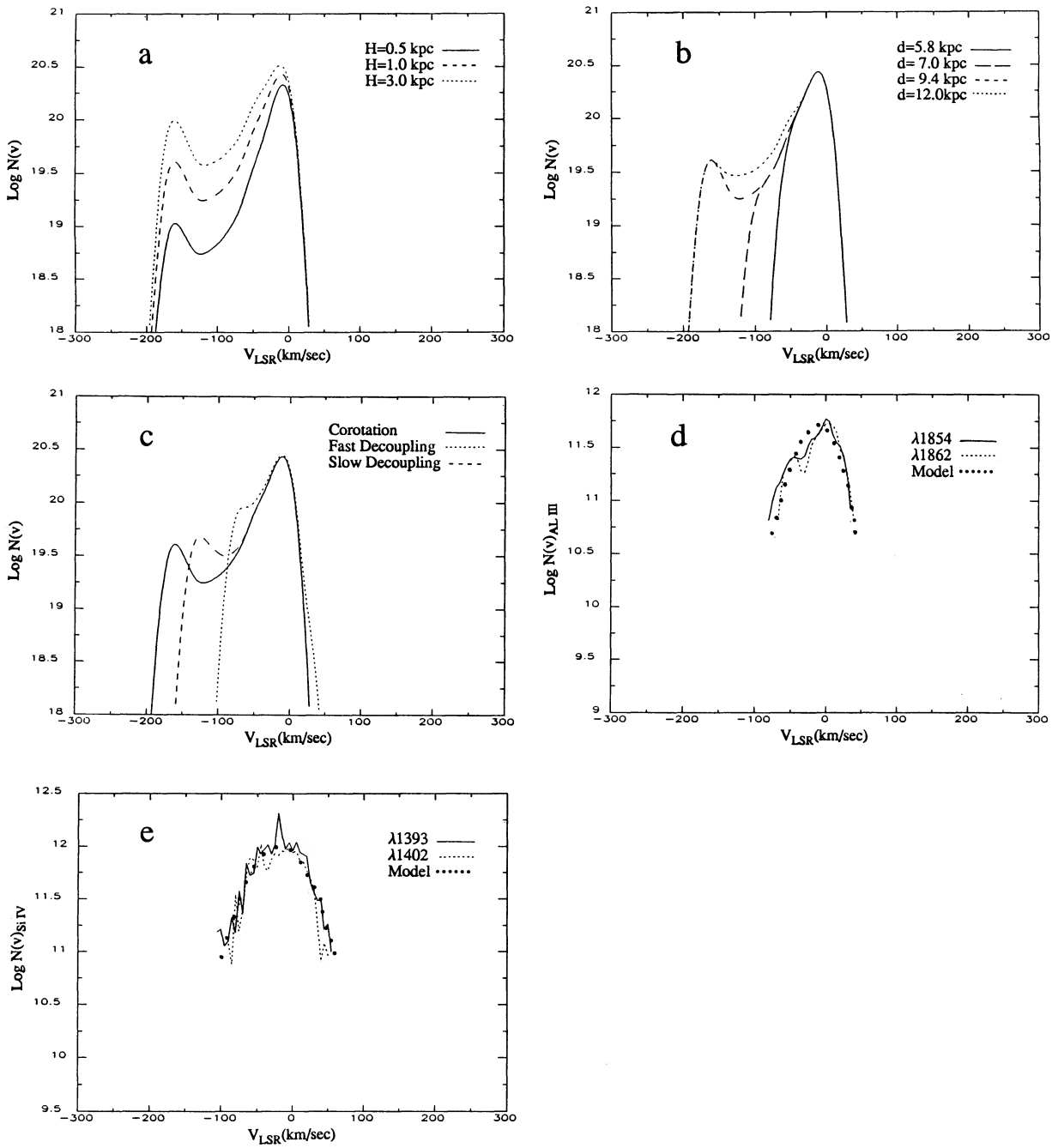

FIG. 7.—(*a*) An illustration of how the scale height, H, of an absorbing species influences the shape of the $N(v)$ vs. v curve. The cases illustrated assume corotation, a velocity dispersion $\sigma = 10$ km s^{-1}, and $H = 3.0$, 1.0, and 0.5 kpc. The assumed distance over which absorption occurs is 9.4 kpc, and the assumed midplane density which establishes the column density scaling on the vertical axis is $n_0 = 1.0$ atom cm^{-3}. (*b*) An illustration of how the line-of-sight distance, d, over which the absorption occurs, influences the shape of the $N(v)$ vs. v curves. The various cases presented are for corotating halo gas with $d = 12$, 9.4, 7.0, and 5.8 kpc. The curves also assume a gas scale height, $H = 1$ kpc; a velocity dispersion, $\sigma = 10$ km s^{-1}; and a midplane density, $n_0 = 1.0$ atom cm^{-3}. (*c*) An illustration of how deviations from corotation influence the shape of the $N(v)$ vs. v curves. The three curves shown are for an assumed distance, $d = 9.4$ kpc; scale height $H = 1$ kpc; and velocity dispersion, $\sigma = 10$ km s^{-1}. The solid line is for corotating halo and disk gas. The long dashed line is for a "slow decoupling" of corotation with $f(|z|)$ linearly decreasing from 1.0 to 0 between $|z| = 1.0$ and 3.0 kpc. The short dashed line is for a "rapid decoupling" of corotation with $f(|z|)$ linearly decreasing from 1.0 to 0 between $|z| = 1.0$ and 1.5 kpc. (*d*) An illustration of an attempt to approximately model the observed $N(v)$ vs. v curves for Al III. The observed curves for the $\lambda\lambda$1854 and 1862 lines from Fig. 4 are shown as the solid and dashed curves, respectively. The model profile shown with the filled circles assumes corotating gas exists to a line-of-sight distance, $d = 6$ kpc; a velocity dispersion, $\sigma = 20$ km s^{-1}; a scale height, $H = 0.7$ kpc; and a midplane density, n_0(Al III) $= 3.2 \times 10^{-9}$ atoms cm^{-3}. Limiting the distance to 6 kpc is equivalent to saying that for $d > 6.0$ kpc there is no Al III included in the model calculation. This is necessary for a corotating model in order to eliminate gas with $v < -75$ km s^{-1}. The model curve was convolved with the *IUE* instrumental function which was taken to be a Gaussian with FWHM = 20 km s^{-1}. (*e*) An illustration of an attempt to approximately model the observed $N(v)$ vs. v curves for Si IV. The observed curves for the $\lambda\lambda$1393 and 1402 lines from Fig. 4 are shown as the solid and dashed curves, respectively. The model profile shown with the open circles assumes corotating gas exists to a line-of-sight distance, $d = 6$ kpc; a velocity dispersion, $\sigma = 30$ km s^{-1}; a scale height $H = 3$ kpc; and a midplane density, n_0(Si IV) $= 1 \times 10^{-8}$ atoms cm^{-3}. Limiting the distance to 6 kpc is equivalent to saying that for $d > 6.0$ kpc there is no Si IV included in the model calculation. This is necessary for the corotating model in order to eliminate corotating gas with $v < -75$ km s^{-1}. The model curve was convolved with the *IUE* instrumental function which was taken to be a Gaussian with FWHM = 20 km s^{-1}. Equally good fits can be obtained with noncorotating models containing gas with $d > 6$ kpc.

distances of 12, 9.4, 7, and 5.8 kpc are shown for $H = 1.0$ kpc and $\sigma = 10$ km s^{-1} in Figure 7*b*. These distances correspond to the star located at $d + \sigma_d$, d, $d - \sigma_d$, and at the edge of the 3 kpc arm (the last-named case simulates setting the gas density to zero inside the 3 kpc arm). For small H, increasing or decreasing the distance has little effect since the position of the star is well beyond the absorbing gas in all cases. For large H, the character of the profile changes dramatically once the distance to the star places it on the near side of the tangent point. Absorption at a particular velocity is proportional to $n(d) \times \Delta d/\Delta v$, where $n(d)$ is the number of atoms cm^{-3} at d (or its equivalent v). For fixed density, the absorption at a particular velocity is inversely proportional to the velocity gradient. Consequently, when the gradient is small, a "bunching" of ions in velocity effectively increases the number of available absorbers. For the closer cases, the effect of velocity "bunching" near the tangent point becomes reduced, and the profile becomes much more sharply peaked toward zero velocity. Increasing the distance to the star also affects only the large scale height cases by slightly increasing the absorption between the tangent point and the central peak.

Experimentation with different galactic rotation curves, such as a flat curve with a constant 220 km s^{-1} rotation velocity, reveals that the choice of other plausible disk rotation curves has only a modest effect for the HD 163522 sight line.

The most dramatic changes in the profile are caused by departures from corotation because relaxing the requirement of corotation changes the position of the tangent point. This is demonstrated by the dashed line in Figure 6 which shows the effect of multiplying the rotation curve by a function $f(|z|)$ defined to be 1.0 for $|z| < 1.0$ kpc, decreasing linearly to 0 at 1.5 kpc, and remaining zero thereafter. The position of the tangent point shifts from $d = 8.5$ to 6.8 kpc and now occurs at a velocity of about -75 km s^{-1} rather than -175 km s^{-1}. The effects of deviations from corotation for two examples are shown in the model profiles of Figure 7*c* for $H = 1.0$ kpc and $\sigma = 10$ km s^{-1}. In the case of the dotted line, the rotational velocity rapidly decreases linearly from the corotation value to zero between $|z| = 1.0$ and 1.5 kpc, while in the case of the dashed line the linear decrease to zero occurs between $|z| = 1.0$ kpc and 3.0 kpc.

We must emphasize that the effects shown in Figure 7*c* apply only to that gas along the line of sight which is above 1 kpc. For the line of sight to HD 163522, this means that they apply *only* to gas more distant than 6.3 kpc, which corresponds to galactocentric radii less than 2.6 kpc, i.e., the innermost regions of the Galaxy.

c) *Discussion of the Optical Depth Profiles for HD 163522*

In this section we discuss the kinematical implications of observed optical depth profiles for the neutral gas (e.g., H I and Fe II), for the moderately ionized gas (e.g., Al III), and for the highly ionized gas (e.g., Si IV, C IV, and N V).

The H I *Emission-Line Profile.*—The observed H I 21 cm emission profile for the sight line to HD 163522 is illustrated in Figure 2 and is replotted at the observed 1 km s^{-1} resolution in logarithmic form in Figure 5*a*. Species strongly confined to the Galactic plane such as H I exhibit profiles much more strongly peaked toward $v_{LSR} = 0$ km s^{-1} than the profiles observed for the highly ionized species (see Fig. 3). The curves in Figure 5*b* illustrate three attempts to model the observed 21 cm profile using the model gas layer described in § VI*a*. The computed curves include the three H I components required by Lockman (1984) to describe the distribution of H I in the inner Galaxy. The three components include two Gaussians and an exponential with midplane densities of 0.16, 0.093, and 0.053 atoms cm^{-3} and scale heights of 106, 254, and 480 pc, respectively. The velocity dispersions we have assumed for the three phases of H I are 5, 10, and 15 km s^{-1}, respectively. The three cases illustrated in Figure 5*b* assume corotating gas in the halo and were calculated for three values of the distance over which the emitting gas might exist, 5.8, 7.0, and 9.4 kpc. According to Lockman (1984) there is an abrupt change in the H I layer at $R = 3.5$ kpc, and neutral halo gas is absent for $R < 3$ kpc. For our sight line, $R = 3.0$ kpc corresponds to a line-of-sight distance of $d = 5.8$ kpc and a Galactic altitude of $z = -0.9$ kpc. Comparing the model curves of Figure 5*b* to the actual observations of Figure 5*a*, we see that, with the exception of an extra narrow emission feature near $+37$ km s^{-1} and a small required velocity shift for the strong local emission, the model curves for $d = 5.8$ and 7.0 kpc bracket the observed profile. In particular, the ledge of emission extending from about -60 km s^{-1} to -90 km s^{-1} shows up in the model for $d = 7.0$ kpc but is missing for $d = 5.8$ kpc. Perhaps this ledge is associated with the relative enhancement in halo H I noted by Lockman (1984) in the region $R = 3$–3.5 kpc.

The Fe II *Profile.*—The composite data for the Fe II absorption lines illustrated in Figure 5*c* have been combined as described in § IV*b* to produce the $N(v)$ curve for Fe II illustrated in Figure 5*d*. For comparison we also show the $N(v)$ curve for H I which has been degraded to the *IUE* instrumental resolution of approximately 20 km s^{-1}. We note that while the Fe II and H I profile shapes agree well over the velocity ranges $+30$ to $+80$ km s^{-1} and -30 to -40 km s^{-1}, the Fe II profile lies significantly higher than the H I profile for $v < -40$ km s^{-1}. One interpretation of this difference is that Fe II has a larger scale height than H I. However, Fe II existing in ionized gas could also produce the difference.

Previous studies of the stratification of refractory elements away from the galactic plane by Edgar and Savage (1989) and van Steenberg and Shull (1988) have shown that the apparent scale height of Fe II is indeed greater than that of H I, a result possibly attributed to the destruction of Fe bearing grains at large distances away from the Galactic plane. This destructive processing may result from the same processes which eject gas to large distances from the galactic plane.

The larger Fe II scale height may also result from a multiphase medium whose components have different scale heights and different depletions (see Edgar and Savage 1989). For an assumed Fe abundance of Fe/H $= 3 \times 10^{-5}$, the data of Figure 5*d* imply a depletion of $\sim 1/30$ for gas with $v > -40$ km s^{-1} and a depletion of $\sim 1/6$ for gas with $v < -40$ km s^{-1}.

Jenkins (1985) has proposed that the enhanced Fe-to-H ratio in gas at large distances from the Galactic plane may be due to the enrichment of Fe in the galactic halo by the ejecta from Type I supernovae. Unfortunately, the present observations cannot discriminate between the various ideas proposed to explain the enhanced Fe/H ratio of halo gas.

The Al III *Profile.*—The Al III profile is shown in Figure 3. For the direction to HD 163522, Galactic rotation is not expected to produce positive velocity shifts; therefore the positive velocity extensions of profiles can be used to estimate the velocity dispersion of the gas. The positive velocity extent of the Al III profile implies a velocity dispersion of 10–20 km s^{-1}. The negative velocity cutoff implies that there is little Al III in gas with velocities < -75 km s^{-1}. For corotating gas, this

corresponds to $d = 6.5$ kpc, $R = 2.4$ kpc, and $z = -1$ kpc. The Al III profile can be approximately modeled by a corotating gas with a scale height of 700 pc, a velocity dispersion of 20 km s^{-1}, and a midplane density which vanishes for line-of-sight distances greater than 6 kpc. This model is compared to the observations in Figure 7*d*. As with Fe II, the required cutoff of corotating Al III–bearing gas for $d > 6$ kpc may be related to the lack of neutral high $|z|$ H I gas for $R < 3.0$ kpc observed by Lockman (1984). However, an inspection of the curves shown in Figure 7*c* reveals that absorption by gas beyond $d = 6$ kpc is possible, provided the gas deviates substantially from corotation.

The Si IV, C IV, *and* N V *Profiles.*—The profiles for Si IV, C IV, and N V, shown in Figure 3, are broader and show stronger absorption at large negative velocities (relative to $v = 0$ km s^{-1}) than do the profiles for H I, Fe II, or Al III. The simplest interpretation of this effect is that we are seeing the consequences of viewing gas in phases with greater scale heights which enhances the absorption by distant gas and accentuates the effects of galactic rotation (see Fig. 7*a*). The positive velocity extents of the observed high-ion profiles imply velocity dispersions of approximately 25–30 km s^{-1}, similar to that found by Jenkins (1978) for O VI in the disk. Allowing for the larger velocity dispersions of these ions, none of the profiles suggest appreciable absorption by gas with rest velocities less than about -75 km s^{-1}. Once again, it is possible to impose a cutoff in the absorbing gas at $R = 3$ kpc and obtain a fit to the observed profiles (see Fig. 7*e*). In this case, however, eliminating all traces of absorbing gas inside the 3 kpc arm poses some rather powerful constraints upon the conditions of the gas in the region, as discussed in the next section.

d) Implications of the Results

The major difference between the observed profiles and those calculated by the simplest model (a corotating gas layer whose scale height and midplane density are independent of R) is that the observed profiles do not show significant absorption at velocities less than -75 km s^{-1}. There are two ways the model can be modified to accommodate this discrepancy. One is to allow the midplane density to vary with R (specificially, to set it to zero inside the 3 kpc arm), and the other is to allow for deviations from corotation in the halo. There are reasons to suspect that one or both of these influences may be affecting the profiles.

If the high ions exist only along the sight line to a distance of about 6 kpc but are corotating with disk gas to that distance, we find that the model calculations can provide an approximate representation of the observed profiles (Fig. 7*e*). Such a model distribution implies that the high-ionization gas is missing inside the 3 kpc arm. This is a reasonable hypothesis since the 1 keV X-ray emission discussed in § IV may emanate from this region, implying that most of the gas interior to the 3 kpc arm is too hot to produce observable quantities of Si IV, C IV, and N V. In particular, Nousek *et al.* (1982) point out that if the observed X-ray emission is from the Galactic center, its emission measure and spectral index imply a gas temperature and density $\sim 3 \times 10^6$ K and $\sim 3 \times 10^{-3}$ atoms cm^{-3}. One way to ensure that nearly all of the gas inside the 3 kpc arm is hot enough to escape detection in the *IUE* ultraviolet measurements is to not allow the gas to remain in the region long enough to cool. This idea is compatible with Bregman's (1980) suggestion that the inner Galaxy may have a wind while the outer Galaxy may have a bound fountain.

If the high ions actually exist along the entire sight line to 9.4 kpc with a substantial scale height (say 3 kpc), then, as Figure 7*c* indicates, there must be major deviations from corotation for $d > 6$ kpc ($v < -75$ km s^{-1}, $R = 2.6$, $|z| > 1$ kpc). The idea that the halo and disk could decouple at such a low altitude may seem to conflict with the results obtained for lines of sight toward extra galactic sources (York *et al.* 1982; D'Odorico, Pettini, and Ponz 1985), which indicate that corotation may persist to much greater altitudes. However, for the HD 163522 line of sight, departures from corotation would be required to occur exclusively inside the 3 kpc arm. By comparison, the closest any of the extragalactic lines of sight studied by these authors comes to the center of the Galaxy is the one toward Mrk 509 whose tangent point is $R = 5$ kpc. Thus, there is no conflict with these previous results as long as we suppose that departures from corotation at such small $|z|$ occur only inside the 3 kpc arm. The result discussed here is related to an *absence* of absorption when it is expected to occur and should not be confused with the well-known result that parcels of gas moving with peculiar velocities are found along many lines of sight. For example, in the vicinity of the Sun there is evidence for motions of distant gas toward the plane with speeds, v_z, of up to 100 km s^{-1} (Albert 1983; Danly 1989). If such gas existed toward HD 163522, it would produce only a small modification of the observed profiles because the line of sight component of motion is small (e.g., 100 sin $|9.^\circ3|$ $\sim$ 16 km s^{-1}). On the larger scale, there is considerable evidence for peculiar motions both in Ca II absorption (Morton and Blades 1986) and in the H I high-velocity cloud phenomena (Kaelble, de Boer, and Grewing 1985). The motions of cooling parcels of gas participating in a Galactic fountain may explain some of these phenomena.

There is a class of models for the 3 kpc arm (van der Kruit 1971; Saunders and Pendergast 1974) in which departures from corotation inside the arm arise quite naturally. In these models, gas with little or no angular momentum is ejected from the Galactic core and then interacts with undisturbed disk gas to create the expanding 3 kpc arm. These models imply that gas inside the 3 kpc arm need not participate in the general rotation of the Galaxy. Although the arm itself acquires considerable angular momentum through its interaction with the disk gas, the same need not be true for gas expanding into the halo. In this context, it is interesting that the observed radial velocity of HD 163522 is nearly the negative of the component of the LSR motion along the line of sight, $-220 \cos(b) \sin(l) = +39$ km s^{-1}, suggesting that the rotational motion of the star about the center of the Galaxy is nearly at rest at its position of 1.5 kpc below the Galactic plane.

So far, we have ignored the possibility of systematic radial inflows or outflows associated with gas at large $|z|$. In the Galactic fountain model (Bregman 1980), the hot (10^6 K) rising fountain gas is expected to have a component of motion radially outward while the cooling fountain gas (e.g., $T < 10^5$ K) is expected to have a component radially inward. In addition to fountain flows, we should also be concerned that our sight line passes over the location of the expanding 3 kpc arm of the disk. The event that produced the 3 kpc arm could have imparted radial outflow to gas in the halo above and below the arm. In the direction $l = 350^\circ$ and $b = 0^\circ$, the 3 kpc arm has a radial velocity of about -110 km s^{-1}, yet there is no evidence in any of the profiles for strong absorption near this velocity. This observation alone indicates that large differences exist (in

either the density or kinematical structure) between the disk and halo gas in the inner regions of the Galaxy.

It is impossible to distinguish between the many possible kinematical interpretations by analyzing a single star. Much of the observed structure in the line profiles may be unique to the line of sight to HD 163522 which penetrates a very interesting region of the Galaxy. We are currently investigating additional lines of sight for stars which pass near, but do not penetrate, the 3 kpc arm in order to establish which kinematical effects are unique to the arm and which are more indicative of the general aspects of the inner halo.

VII. THE ORIGIN OF THE HIGHLY IONIZED GAS

The absorption line data shown in Figure 2 and the plots of optical depth versus velocity in Figures 3 and 4 provide insights into the origin of the highly ionized gas in the Galactic disk and halo. Of great significance is the definite detection of N v absorption in the λ1238 line whose optical depth profile resembles that of C IV and Si IV. The significance of N v is that among the highly ionized species that can be studied by *IUE*, it is the most difficult to produce. Since most hot stars have strong 54 eV He^+ absorption edges and because the conversion of N IV into N v requires 77 eV, it is difficult to identify sources that might produce N v by photoionization. Thus, the N v lines represent the best diagnostic of the hot ISM available in the *IUE* wavelength range.

Theories of the origin of the highly ionized gas found at large distances away from the Galactic plane must explain both the support of the gas and the ionization of the gas. The competing theories for the support of the gas are the cosmic-ray–supported halo models (Hartquist, Pettini, and Tallant 1984; Chevalier and Fransson 1984; Hartquist and Morfill 1986) and the Galactic fountain models (Shapiro and Field 1976; Bregman 1980). In the cosmic-ray–supported halo models, the ionization of the gas is provided by energetic photons from hot white dwarfs (Dupree and Raymond 1983), normal Population I stars, and from the extragalactic EUV background. In Galactic fountain models, the ionization is associated with cooling collisionally ionized intermediate temperature (0.8 to 3×10^5 K) gas participating in the fountain flow (Edgar and Chevalier 1986).

Several detailed calculations have been performed to estimate the expected amounts of Si IV, C IV, and N v in photoionized halo models (Hartquist, Pettini, and Tallant 1984; Chevalier and Fransson 1984; Fransson and Chevalier 1985; Bregman and Harrington 1986). Results from one of these calculations are given in Table 4 along with values of N(ion) $|\sin b|$ for the average sight line through the halo based on the results of Savage and Massa (1987), for the sight line to SN 1987A in the LMC (Savage *et al.* 1989), for HD 5980 in the SMC (Fitzpatrick and Savage 1983), and for HD 163522. The predicted ionic column density ratio of N v to C IV in the photoionized halo model listed is 0.0061 compared to the observed value of N(N v)/N(C IV) = 0.38, a factor of 62 difference. While other model calculations differ in detail depending on such assumptions as the density distribution of the gas and the nature of the ionizing background assumed, none of the available models comes within a factor of 10 of the observed N v to C IV abundance ratio. Although a relatively high level of ionization can be achieved by letting the ratio of gas density to ionizing photon density become very small, those models that give the proper ratio of N v to C IV have such low gas densities that distances much larger than the one to HD 163522 are required to build up the observed column density. In contrast to the photoionized halo models, the cooling fountain flow calculations of Edgar and Chevalier (1986) for a fountain mass flow rate of 4 $M_\odot$ yr^{-1} do provide N v and C IV column densities and ionic abundance ratios compatible with the observations (see Table 4). However, as pointed out by Savage *et al.* (1989) for the sight line to SN 1987A, these calculations fall short by about a factor of 4 or 5 in explaining the observed column density of Si IV. The same problem holds for

TABLE 4

COLUMN DENSITIES FOR HIGHLY IONIZED MILKY WAY HALO GAS

Ion	Photoionized Halo[a] $N \lvert\sin b\rvert$	Cooling Fountain[b] $N \lvert\sin b\rvert$	Halo Stars[c] $\langle N \lvert\sin b\rvert\rangle$	HD 5980[d] $N \lvert\sin b\rvert$	SN 1987A[e] $N \lvert\sin b\rvert$	HD 163522[f] $N \lvert\sin b\rvert$
Al III	...	...	...	4.5×10^{12}	7.3×10^{12}	5.4×10^{12}
Si IV	1.3×10^{14}	$(3.3 - 6.4) \times 10^{12}$	$\approx 2 \times 10^{13}$	2.8×10^{13}	1.9×10^{13}	1.4×10^{13}
C IV	1.2×10^{14}	$(4.3 - 7.9) \times 10^{13}$	$\approx 1 \times 10^{14}$	1.8×10^{14}	7.7×10^{13}	5.6×10^{13}
N v	7.3×10^{11}	$(2.8 - 3.6) \times 10^{13}$	$\approx 3 \times 10^{13}$	2.2×10^{13}	...	2.1×10^{13}
O VI	1.4×10^{11}	$(5.8 - 6.0) \times 10^{14}$	$> 3 \times 10^{13}$	...	...	...

[a] Predicted column densities of highly ionized gas through the halo ($N \lvert\sin b\rvert$) based on the cosmic-ray–supported photoionized halo calculations of Hartquist, Pettini, and Tallant 1984. The model values listed are for the model in which the warm 10^4 K gas has a large filling factor and a large pressure scale height with $n_0 = 3 \times 10^{-3}$ cm^{-3} and $H = 3$ kpc. Note that the photoionized models produce very little N v and O VI.

[b] Predicted column densities of highly ionized gas through the halo ($N \lvert\sin b\rvert$) on one side of the galaxy based on the time-dependent ionization calculations of Edgar and Chevalier 1986. The values assume a fountain mass flow rate of 4 $M_\odot$ yr^{-1} on each side of the Galactic plane. The two values of $N \lvert\sin b\rvert$ listed for each ion involve different assumptions about the sizes of the cooling regions. These same calculations explain the C IV and O III emission measurements of Martin and Bowyer 1990 provided the fountain mass flow rate is about two times larger than assumed above.

[c] Observations are from Savage and Massa 1987 for Si IV, C IV, and N v and from Jenkins 1978 for O VI. The value for O VI is listed as a lower limit because the measures only extend to $|z| \approx 1$ kpc.

[d] The values listed are for the sight line to HD 5980 in the SMC from Fitzpatrick and Savage 1983 and refer to gas with $v < 100$ km s^{-1}.

[e] The listed column densities are for gas in the direction of SN 1987A with $v < 120$ km s^{-1} from Savage *et al.* 1989.

[f] The values of $N \lvert\sin b\rvert$ listed for HD 163522 are obtained from an average of the values of N(ion) listed in Table 3. Since the z of HD 163522 is -1.5 kpc which is smaller than the estimated scale heights of Si IV, C IV, and N v, one might expect the values of $N \lvert\sin b\rvert$ for the extragalactic objects to exceed those for HD 163522.

the sight line to HD 163522 where the observed ratio of column densities of Si IV to C IV is 0.25 while the value predicted for cooling fountain gas is 0.08. While one could argue that a combination of processes (i.e., photoionization and cooling fountain) may be influencing these ratios, we note that the observed profiles for N V, C IV, and Si IV toward HD 163522 are quite similar in shape, suggesting that a common process may be responsible for creating the three ions.

There is another aspect of the data shown in Figures 2, 3, and 4 which casts doubt on the validity of models which attribute the highly ionized species to halo gas photoionized by an extragalactic EUV radiation field. Such models predict a large increase in n(ion) for Si IV and C IV near $|z| \approx 1$ kpc (Hartquist, Pettini, and Tallant 1984; Fransson and Chevalier 1985). While one can imagine that a factor of 2 or 3 increase in $N(\text{ion})|\sin b|$ versus $|z|$ near $|z| = 1$ kpc can be seen in the plots of Savage and Massa (1987) for Si IV and C IV and that an even larger increase may be present in the data presented by Pettini and West (1982), we can ask what effect such an enhancement would have on the Si IV and C IV profiles for the sight line to HD 163522. In the direction to HD 163522, $z = -1$ kpc occurs at a line-of-sight distance of 6.3 kpc. Corotating halo gas at that distance has $v_r = -75$ km s^{-1} according to the rotation law shown in Figure 6. If there were very little Si IV and C IV between the Sun and $d = 6.3$ kpc followed by a substantial jump in n(Si IV) and n(C IV), at that distance we would expect the Si IV and C IV profiles to have relative maxima near $v = -75$ km s^{-1}. In contrast, the actual profiles are quite broad with absorption half widths extending from about $+30$ to -80 km s^{-1}. However, as discussed in § VI, the presence of the 3 kpc arm may be affecting the observed profiles. Clearly, similar studies for additional sight lines will be valuable.

VIII. SUMMARY

The principal results of our study of the high signal-to-noise ratio *IUE* high-dispersion UV data we have obtained for HD 163522 are as follows:

1. The UV stellar spectrum of HD 163522 is consistent with the star being a normal B1 Ia star with $M_v = -7.0 \pm 0.5$ mag and at a distance of $9.4^{+2.4}_{-1.9}$ kpc. With $l = 349.^{\circ}6$ and $b = -9.^{\circ}1$, the estimated distance implies the star is located beyond the Galactic center and 1.5 kpc below the Galactic plane. Its large peculiar radial velocity of -172 km s^{-1} suggests that the star is not participating in Galactic rotation.

2. The UV interstellar absorption lines from species formed in the neutral, weakly ionized, and highly ionized gas are very strong and broad. The lines show asymmetrical extensions to $v_{\rm LSR} \approx -100$ km s^{-1}.

3. The observed absorption line profiles for Al III, Si IV, C IV, and N V have been converted into plots of optical depth versus velocity. A comparison of such plots for the weak and strong member of the Al III and Si IV doublets reveals that the lines are not influenced by unresolved saturated components. Therefore, the observed optical depth profiles can be directly converted into measures of $N(v)_{\rm X}$, the column density of species X per unit velocity interval.

4. The derived profiles are strongly influenced by the effects of Galactic rotation over the enormous distance to HD 163522. Those species known by independent studies to have very large scale heights (e.g., Si IV, C IV, and N V) show significantly more high velocity absorption than species which are more confined to the Galactic plane (e.g., H I, Fe II, Mg II, S II, etc.). This result is a natural consequence of the larger scale height gas enhancing the contribution by distant gas thereby accentuating the effects of Galactic rotation on the profiles.

5. Substantial differences in the profile shapes for H I and Fe II imply that Fe is considerably less depleted in gas with $v < -40$ km s^{-1} than it is in gas with $v > -40$ km s^{-1}.

6. Although the sight line passes over the expanding 3 kpc arm at a z distance of about -0.9 kpc, we find no evidence for absorption at velocities which are characteristic of the arm in the underlying disk for the direction $l = 350^{\circ}$.

7. An analysis of the observed profile shapes shows that they do not conform with those expected for the simplest kinematical model of corotating halo gas with a scale height and a midplane density for each species that is independent of R. Departures from such a simple model may be due to either an absence of gas, including the high ionization species for $R < 3$ kpc, or to departures from corotation for gas with $R < 3$ kpc. In either case, it is clear that even though the integrated properties of the innermost regions of the gaseous halo are similar to local ones (Savage and Massa 1985), the structural details are quite complex.

8. Integration of the optical depth profiles for N V, C IV, Si IV, and Al III over the velocity range from -100 to $+60$ km s^{-1} yields total column densities of $\log N = 14.09$, 14.55, 13.96, and 13.53, respectively. These values can be compared to $\log N(\text{H I}) = 21.04$, based on the strength of the damped Lyman-α absorption line.

9. The definite detection of strong N V absorption with a profile shape similar to those of C IV and Si IV favors the view that the origin of these features is in collisionally ionized intermediate-temperature gas associated with the nonequilibrium time dependent cooling of gas in a Galactic fountain.

10. Although the observed N V and C IV column densities are compatible with the time-dependent ionization calculations of Edgar and Chevalier (1986) for a fountain flow with a mass circulation rate of about 4 $M_\odot$ yr^{-1} on each side of the Galactic plane, the predicted column density of Si IV is about 4 times smaller than observed.

11. This research has established that a wealth of information exists in UV absorption-line profiles obtained for sight lines where a Galactic rotation curve can be used to estimate the distance of the absorbing matter.

We thank the *IUE* observatory staff at the Goddard Space Flight Center for their help in acquiring and processing the *IUE* data for HD 163522. We acknowledge valuable discussions regarding halo gas and data reduction techniques with R. Edgar and J. Cardelli. The display and analysis of the spectra were done on the computing facilities of the Midwest Astronomical Data Reduction and Analysis Facility. This work was supported through NASA grants NAG-186 to B. D. S. and NAS 5-29301 to D. M.

REFERENCES

Albert, C. E. 1983, *Ap. J.*, **272**, 509.
Boggess, A. *et al.* 1978*a*, *Nature*, **275**, 372.
———. 1978*b*, *Nature*, **275**, 377.
Bregman, J. N. 1980, *Ap. J.*, **236**, 577.
Bregman, J. N., and Harrington, P. J. 1986, *Ap. J.*, **309**, 833.
Burton, W. B. 1985, *Astr. Ap. Suppl.*, **62**, 365.

Chevalier, R. A., and Fransson, C. 1984, *Ap. J. (Letters)*, **279**, L43.
Clemens, D. P. 1985, *Ap. J.*, **295**, 422.
Courtes, G. 1972, *Vistas Astr.*, **14**, 81.
Danly, L. 1989, *Ap. J.*, **342**, 785.
Danly, L., Savage, B. D., Lockman, J., and Meade, M. 1990, in preparation.
D'Odorico, S., Pettini, M. and Ponz, D. 1985, *Ap. J.*, **299**, 852.
Dupree, A. K., and Raymond, J. C. 1983, *Ap. J. (Letters)*, **275**, L71.
Ebbets, D. C., and Savage, B. D. 1982, *Ap. J.*, **262**, 234.
Edgar, R. J., and Chevalier, R. A. 1986, *Ap. J. (Letters)*, **310**, L27.
Edgar, R. J., and Savage, B. D. 1989, *Ap. J.*, **340**, 762.
Fitzpatrick, E. L., and Savage, B. D. 1983, *Ap. J.*, **267**, 93.
Fransson, C., and Chevalier, R. A. 1985, *Ap. J.*, **296**, 35.
Garrison, R. F., Hiltner, W. A., and Schild, R. E. 1977, *Ap. J. Suppl.*, **35**, 111.
Hartquist, T. W., and Morfill, G. E. 1986, *Ap. J.*, **311**, 518.
Hartquist, T. W., Pettini, M., and Tallant, A. 1984, *Ap. J.*, **276**, 519.
Jenkins, E. B. 1978, *Ap. J.*, **220**, 107.
———. 1985, in *Proc. of the NRAO Conference on Gaseous Halos of Galaxies*, ed. J. N. Bregman and F. J. Lockman (Green Bank: NRAO), p. 1.
Kaelble, A., de Boer, K. S., and Grewing, M. 1985, *Astr. Ap.*, **143**, 408.
Kurucz, R. L., and Peytremann, E. 1975, *Smithsonian Ap. Obs. Spec. Rept.*, No. 362.
Lockman, F. J. 1984, *Ap. J.*, **283**, 90.
Luo, D., Pradhan, A. K., and Shull, M. J. 1988, *Ap. J.*, **335**, 498.
Massa, D. 1989, *Astr. Ap.*, **224**, 131.
———. 1990, in preparation.
Martin, C., and Bowyer, S. 1990, *Ap. J.*, **350**, 242.
McCammon, D., Burrows, D. N., Sanders, W. T., and Kraushaar, W. L. 1983, *Ap. J.*, **269**, 107.
Morton, D. C., and Blades, J. C. 1986, *M.N.R.A.S.*, **220**, 927.
Morton, D. C., and Smith, W. H. 1973, *Ap. J. Suppl.*, **26**, 333.
Nousek, J. A., Fried, P. M., Sanders, W. T., and Kraushaar, W. L. 1982, *Ap. J.*, **258**, 83.
Pettini, M., and West, K. A. 1982, *Ap. J.*, **260**, 561.
Oort, J. 1977, *Ann. Rev. Astr. Ap.*, **15**, 295.
Rickard, J. J. 1974, *Astr. Ap.*, **31**, 47.
Saunders, R. H., and Pendergast, K. H. 1974, *Ap. J.*, **188**, 489.
Savage, B. D., and Massa, D. 1985, *Ap. J. (Letters)*, **295**, L9.
———. 1987, *Ap. J.*, **314**, 380.
Savage, B. D., Jenkins, E. B., Joseph, C. L., and de Boer, K. S. 1989, *Ap. J.*, **345**, 395.
Shapiro, P. R., and Field, G. B. 1976, *Ap. J.*, **205**, 762.
Shull, J. M., van Steenberg, M. E., and Seab, C. G. 1983, *Ap. J.*, **271**, 408.
Thompson, R. W., Turnrose, B. E., and Bohlin, R. C. 1982, *Astr. Ap.*, **107**, 11.
Turnrose, E. B., and Thompson, R. W. 1984, *IUE Image Processing Information Manual Version 2.0* (Computer Science Corp: TM-84/6058).
van der Kruit, P. C. 1971, *Astr. Ap.*, **13**, 405.
van Steenberg, M. E., and Shull, J. M. 1988, *Ap. J.*, **330**, 942.
Walborn, N. R. 1972, *A.J.*, **77**, 312.
———. 1976, *Ap. J.*, **205**, 419.
Walborn, N. R., and Nichols-Bohlin, J. 1987, *Pub. A.S.P.*, **99**, 40.
Walborn, N. R., and Panek, R. J. 1985, *Ap. J.*, **291**, 806.
Wollaert, J. P. M., Lamers, H. J. G. L. M., and de Jager, C. 1988, *Astr. Ap.*, **194**, 197.
York, D. G., Blades, J. C., Cowie, L. L., Morton, D. C., Songaila, A., and Wu, C. C. 1982, *Ap. J.*, **255**, 467.

DERCK MASSA: Applied Research Corporation, Suite 920, 8201 Corporate Drive, Landover, MD 20785

BLAIR D. SAVAGE and KENNETH SEMBACH: Washburn Observatory, Department of Astronomy, University of Wisconsin, 475 North Charter Street Madison, WI 53706